Journal of Alloys and Compounds 1002 (2024) 175273

Contents lists available at ScienceDirect

Journal of Alloys and Compounds

journal homepage: www.elsevier.com/locate/jalcom

Solid solution strengthening in single-phase Au-Cu-Ni-Pd-Pt-based high-entropy alloys

S. Drescher [a,b], S. Seils [c], T. Boll [c], A. Kauffmann [c], M. Heilmaier [c], J. Freudenberger [a,b,*]

[a] Leibniz Institute for Solid State and Materials Research Dresden, Helmholtzstr. 20, Dresden 01069, Germany
[b] TU Bergakademie Freiberg, Institute of Materials Science, Gustav-Zeuner-Str. 5, Freiberg 09599, Germany
[c] Karlsruhe Institute of Technology (KIT), Institute for Applied Materials (IAM-WK) and Karlsruhe Nano Micro Facility (KNMF), Engelbert-Arnold-Str. 4, Karlsruhe D-76131, Germany

ARTICLE INFO

Keywords:
Solid solution strengthening
High-entropy alloys
Mechanical properties
Precious metals

ABSTRACT

The Au-Cu-Ni-Pd-Pt system is an ideal benchmark system to investigate the composition-dependent effect on solid solution strengthening in multi-element alloys, in particular high-entropy alloys. It allows studying the strength for deliberately adjusted compositional variations without any phase transformations taking place. In this study, alloy series are produced, in which one element is gradually replaced by another while these two elements are additionally alloyed to an equimolar three-element solid solution. The variations in concentration x are as follows: $Au_xNi_{25-x}(CuPdPt)_{75}$ and $Ni_xPt_{25-x}(AuCuPd)_{75}$ (x = 0, 5, 10, 15, 20, 25 at%). A non-linear trend of strength vs. concentration x is observed with maximum values close to the equimolar ratio of the two interchanged elements. The observed behavior cannot be explained by the commonly accepted model for solid solution strengthening of Varvenne and co-workers [1]. Possible reasons for the discrepancy between model and experiment are critically discussed.

1. Introduction

Single-phase, multi-element alloys containing five or more elements with molar concentrations between 5 and 35 at% of each element are known as High-Entropy Alloys (HEAs) [2,3]. Among them, CoCrFeMnNi attracted the interest of researchers due to its high strength and large ductility, which both increase with decreasing temperature [4–6]. As for CoCrFeMnNi, it is widely assumed that solid solution strengthening is the dominant strengthening mechanism in HEAs for two reasons: (i) single-phase alloys in the recrystallized, coarse-grained state barely show other strengthening mechanisms such as dislocation strengthening and grain boundary strengthening. (ii) these single-phase alloys consist of a large amount of different constituent elements which results in complex dielastic and parelastic dislocation interactions. Conventional models describing the solid solution strengthening cannot be easily transferred to HEAs. Such models only consider small amounts of solute elements (< 10 at% Labusch [7], < 2 at% Fleischer [8]). Concerning the HEAs, no solvent element can be identified, since the solid solution is constituted of several elements in similar proportions. However, in order to facilitate the design of engineering materials, a fundamental understanding of the physical metallurgy of HEAs is required. In particular, it is necessary to develop reliable models for the prediction of their mechanical properties. Such models require a sound and profound experimental database for evaluation and verification. In other words, experimental work is needed that illustrates the composition-dependent solid solution strengthening of different alloys over a preferably large compositional range. The most advanced and widely accepted model for the strength of HEAs was derived by Varvenne et al. [1,9]. This model can be considered as an extension of Labusch's weak-pinning model [7] as it is based on elastic solute-dislocation interactions. A key assumption is that the elements are randomly distributed on the lattice site building an effective matrix in which each atom is considered as a solute; the limitations of the statistical treatments of Labusch's work are effectively mitigated. As a consequence, the strength does not directly depend on the number of elements and their concentration but is determined by the concentration-weighted mean-square misfit volume and the concentration-weighted shear modulus. In the reduced form of Varvenne's model [1], the contribution of solid solution strengthening to the critical shear stress $\Delta\tau_{c,ss}$ can be expressed by Eq. (1) and (2):

* Corresponding author at: Leibniz Institute for Solid State and Materials Research Dresden, Helmholtzstr. 20, Dresden 01069, Germany.
E-mail address: j.freudenberger@ifw-dresden.de (J. Freudenberger).

https://doi.org/10.1016/j.jallcom.2024.175273
Received 15 December 2023; Received in revised form 22 May 2024; Accepted 19 June 2024
Available online 20 June 2024

$$\Delta\tau_{c,ss}(T,\dot{\varepsilon}) = \frac{0.0178 \quad \overline{G} \quad \vartheta}{\alpha^{\frac{1}{3}}} \cdot \left[1 - \left(\frac{k_B T}{1.5618 \quad \alpha^{\frac{1}{3}} \quad \overline{G} \quad b^3 \vartheta} \ln\left(\frac{\dot{\varepsilon}_0}{\dot{\varepsilon}}\right)\right)^{\frac{2}{3}}\right] \tag{1}$$

$$\vartheta = \left(\frac{(1+\overline{\nu})}{(1-\overline{\nu})}\right)^{\frac{2}{3}} \left[\frac{\sum_i x_i \Delta V_i^2}{b^6}\right] \tag{2}$$

With G: the shear modulus,ν: the Poisson ratio, x_i: concentration of the alloying element i, ΔV_i: misfit volume $\Delta V_i = V_i - \overline{V}$, b: length of the Burgersvector, T: temperature, k_B: Boltzmann constant, and $\dot{\varepsilon}$: strain rate. The model assumes that the moduli and lattice parameter of the solution can be estimated upon linear rule of mixtures by taking the values of the elements, i.e. Young's modulus $\overline{E} = \sum_i x_i \quad E_i$, $\overline{G} = \sum_i x_i \quad G_i$. The Poisson's ratio is determined upon $\overline{\nu} = \overline{E}/(2\overline{G} - 1)$. The values of the elastic moduli as well as the lattice parameter of the elements were taken from [10] (see Appendix A1). The so-called key misfit parameter δ is determined according to Eq. (3). According to the model, this parameter is adjusted by varying compositions, and, thus, the strength can be controlled.

$$\delta = \sqrt{\sum_i x_i \Delta V_i{}^2 / 9b^6} \tag{3}$$

The atomic volume of element i and the Burgers vector were determined by $V_i = a_i{}^3/4$ and $b = \frac{\sqrt{2}}{2} a_i$ (a: lattice constant) and the average volume by $\overline{V} = \frac{1}{4}(\sum_i x_i \quad a_i)^3$. In addition, consistent to Varvenne and Curtin [15], the following parameters were taken as $\alpha = 0.123$, $\dot{\varepsilon} = 10^{-3}$ s^{-1}, $\dot{\varepsilon}_0 = 10^4$ s^{-1} and $T = 300$ K. The calculated $\Delta\tau_{c,ss}$ is multiplied by a Taylor factor of 3.06 to express $\Delta\sigma_{c,ss}$ which would represent the contribution of solid solution strengthening to the experimentally observed yield strength in polycrystalline samples with random crystallographic texture. For the CoCrFeMnNi alloy and its face-centered cubic (fcc) subtypes, it has been proven that the experimental yield strength is in satisfying agreement with the predicted values for the contribution of solid solution strengthening to the total strength, which also hints that other strengthening mechanisms are negligible and that the intrinsic strength[1] is low [1,6,12–14]. Likewise, the strength of CoCrFeNiPd could be reasonably described by the model despite nanometer-scaled fluctuations in the composition being observed [15,16]. The model also accomplished a good agreement with the experimental yield strength σ_y for CuNiIrRhPdPt[17].

Significant research has been conducted on equi-atomic alloys. However, there has been limited exploration into the impact of solid solution strengthening in alloys intentionally tailored with non-equimolar compositions, subject to specific concentration variations. This methodical approach serves as a key tool to build-up a reliable dataset for the strength of solid solutions that permit a wide range of variations in composition, ideally encompassing the entire compositional space. This flexibility is essential for thoroughly assessing how models for solid solution strengthening perform. The Au–Cu–Ni–Pd–Pt alloys meet these requirements in a unique manner as they exist as single-phase alloys, and their homogeneous solid solutions cover the entire compositional space, including individual elements, binary, ternary, quaternary, and notably quinary alloys [18,19]. The model of Varvenne [1,9] fails to accurately describe the development of the yield strength in most of the previously investigated Au-Cu-Ni-Pd-Pt alloy series [20,21]. In these series, a fifth element is gradually alloyed to a four-element solid solution. In four out of five series in the manner of $A_x(BCDE)_{100-x}$ (x = 0, 1, 3, 5, 10, 15, 20 at%), a discrepancy between theory and experiment was found. A, B, C, D, and E represent one of the elements Au, Cu, Ni, Pd, and Pt. These series show a linear trend of $\sigma_y(x)$. However, it can be questioned whether the key misfit parameter δ of Varvenne's model [1,9] meets its demands and whether the assumptions on $\overline{E}$ and $\overline{G}$ are justified and applicable. The model reveals that the stacking fault energy has little influence on the strength [1,9], but it does not consider the local chemical surrounding, i.e. short-range order. However, this aspect is neglected here as it affects yield strength only to a minimal extent as stated by Li et al. [1,22]. Otherwise, to rule out that the observed discrepancies between experiment and model are an artefact of the variation of a sole element on the backdrop of a multi-element alloy, further series that vary more than one element must be taken into consideration as well. If this is the case, then a series, in which two elements are exchanged against each other on the backdrop of a three-element alloy ($A_xB_{25-x}(CDE)_{75}$), should not show a linear trend of $\sigma_y(x)$, but rather a course that is known for binary alloys following a parabola-like course.

The model of Varvenne [1,9] is applied to generate $\sigma_y(x)$ data for such series and to reveal peculiarities of depicted series. All series are shown in Appendix 2, Fig. A1. For this study, the series Au_xNi_{25-x}-$(CuPdPt)_{75}$, and $Ni_xPt_{25-x}(AuCuPd)_{75}$ were chosen. The calculated values of $\Delta\sigma_{c,ss}$ show a parabolic dependency on the exchange of Ni by Au (Fig. 1(a)) and an almost linear dependency on the exchange of Pt by Ni (Fig. 1(c)).

$\Delta\sigma_{c,ss}$ is further visualized in dependency on the key misfit parameter (Fig. 1(b), (d)). While there is a nearly linear dependence of $\Delta\sigma_{c,ss}(\delta)$ for $Ni_xPt_{25-x}(AuCuPd)_{75}$ (Fig. 1(d)), no unambiguous relation of $\Delta\sigma_{c,ss}(\delta)$ can be observed for $Au_xNi_{25-x}(CuPdPt)_{75}$ (Fig. 1(b)). The model predicts two different strength values for the same misfit parameter. This is surprising since it is widely accepted that there should be a clear assignment of the key misfit parameter δ to the strength contribution of solid solution strengthening [13,16,23]. Although well working for Co-Cr-Fe-Ni-Mn alloys [1], this assumption might be too simplified in the present case. It is questionable if the key misfit parameter δ is appropriate in its present form when the atomic radii of the constituting elements differ significantly and if the assumption of a linear scaling of the shear modulus is correct. The pronounced deviation from a monotonic $\sigma_y(x)$ trend in combination with the non-unambiguous relationship of $\Delta\sigma_{c,ss}(\delta)$ represents the motivation to select the $Au_xNi_{25-x}(CuPdPt)_{75}$ alloy series for further investigation and evaluate the results against those from the $Ni_xPt_{25-x}(AuCuPd)_{75}$ series, which are supposed to yield a monotonic behavior.

2. Methods

2.1. Processing

Two alloy series of $Ni_xPt_{25-x}(AuCuPd)_{75}$ (x = 0, 5, 10, 15, 20, 25 at%) and $Au_xNi_{25-x}(CuPdPt)_{75}$ (same concentrations and additionally x = 2.5, 7.5 at%) were processed from pure elements with a purity of Au: 4 N, Pd: 3N5, Pt: 4 N (Allgemeine Gold- und Silberscheideanstalt AG), Cu: 5N5 (VEB Spurenmetalle Freiberg/Sa.) and Ni: 4 N (Alfa Aesar). The series were made from ternary master alloys of CuPdPt and AuCuPd to ensure their constant ratio. The two additional elements were further added to pieces of the master alloy in different concentrations. All masses were weighed according to the stoichiometric composition of the desired alloy and melted under Ar atmosphere on a water-cooled Cu plate in an arc furnace (Arc Melter AM 200 Edmund Buehler GmbH). To enhance the homogeneity of the samples, they were flipped over and melted again four times. Finally, the samples were cast into a graphite mould (4 mm in diameter and 75 mm in length). The samples were homogenized at a homologous temperature of approx. 0.9 in sealed quartz ampules under Ar atmosphere and quenched in ice water. Afterwards, the samples were deformed by rotary swaging (UR2–4,

[1] as Hull and Bacon [11] stated, the intrinsic strength τ_0 is a constant stress of uncertain origin.

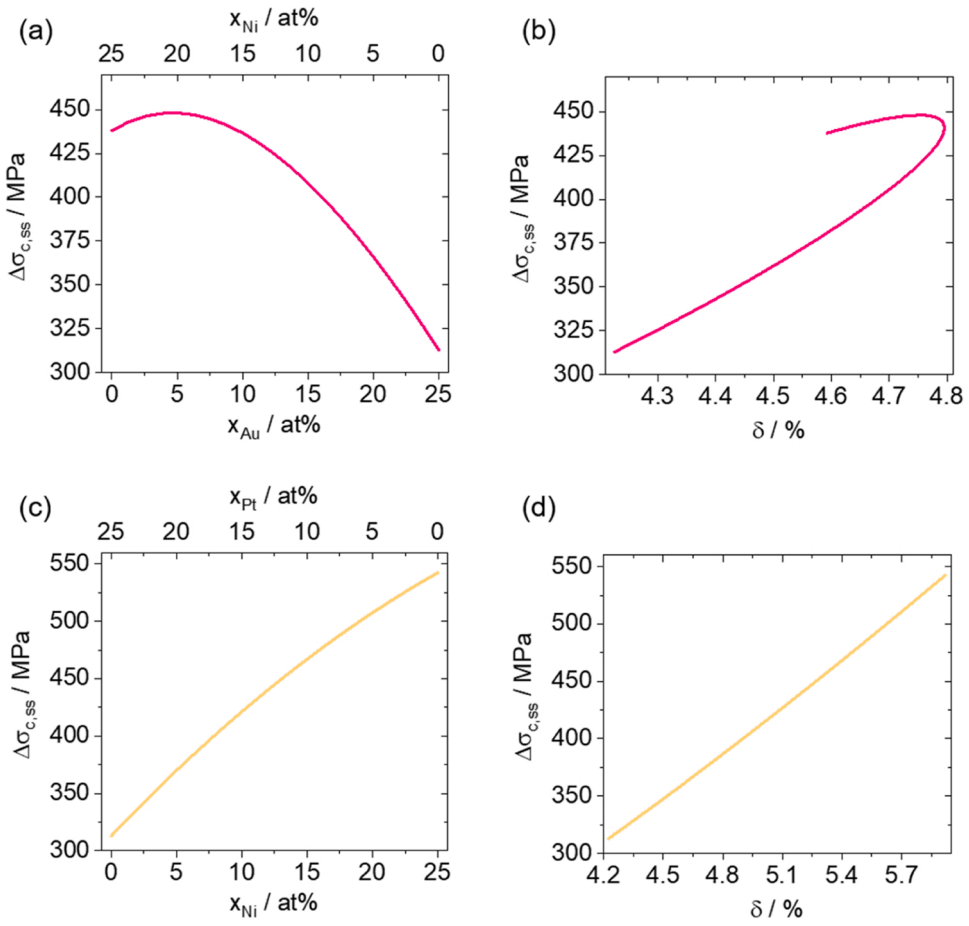

Fig. 1. Calculated contribution of solid solution strengthening to the yield strength in dependence of the concentration (a), (c), and on the misfit parameter δ (b), (d). (a), (b) represent the theoretical interrelation for the series $Au_xNi_{25-x}(CuPdPt)_{75}$; (c), (d) for the series $Ni_xPt_{25-x}(AuCuPd)_{75}$.

Heinrich Müller Maschinenfabrik, Pforzheim) up to a true strain of $\varepsilon = 0.71$ ($\varepsilon = \ln(A_i/A_f)$, where A_i and A_f are the initial and final cross-section area, respectively), while the degree of deformation per step was $\varepsilon \approx 0.24$. Recrystallization heat treatment was done for one hour at the same temperature as the homogenization treatment with subsequent quenching in ice water to maintain the single-phase microstructure [18].

2.2. Characterization methods

Metallographic sample preparation including grinding and diamond polishing down to particle size of 0.25 μm was done according to Ref. [18]. Microstructural characterization was carried out using back-scattered electron imaging (BSE) in an FIB Helios 600i at 10 kV and 1.4 nA. The grain size was determined by the intercept length method including recrystallisation twins (Imagic IMS software). Structural characterization was carried out by X-ray diffraction (XRD) in Debye-Scherrer geometry on bulk samples (≅ 30 μm thickness). For this purpose, a STOE STADI_P diffractometer using $MoK_{\alpha 1}$ radiation and equipped with a position sensitive detector, Dectris Mythen 1 K, as well as a curved Ge(111)-monochromator was used. The scans were taken in the range of 15–60° with a step size of $\Delta\theta = 0.01°$. The lattice parameters of all samples were determined by Rietveld refinement (space group no. 225, $Fm\bar{3}m$ structure model according to Ref. [24]). For atom probe tomography (APT) measurements, a local electrode atom probe was utilized (LEAP 4000X HR, Cameca), operating at a temperature of 50 K, a pulse frequency of 125 kHz and a laser pulse energy of 50 pJ. The sample tips were lifted out within one grain by FIB FEI Strata according to Ref. [25,26]. Data analysis was performed with Cameca IVAS 3.6.14 software. Inductively coupled plasma optical emission spectrometry (ICP-OES) was used to prove the composition of some selected samples after dissolving in aqua regia. Compression tests were carried out with an electro-mechanical Instron 8562 test rig at an initial strain rate of 10^{-3} s^1 on samples of 2.8 mm in diameter and approx. 5.5 mm in height. Yield strength σ_y was obtained as offset yield strength at 0.2 % plastic strain. Microhardness was measured with a Shimadzu HMV-2 hardness tester, a load of 1.98 N, and a dwell time of 10 seconds, while averaging 15 measurements per sample and avoiding indentation positions close to grain boundaries. It is important to highlight that all results presented in this study pertain to the characterization of samples in their recrystallized state.

3. Results and discussion

The present article seeks to assess the solid solution strengthening in selected Au-Cu-Ni-Pd-Pt HEA series by intentionally modifying their composition. The composition of the alloys stands out as the pivotal factor in this evaluation. The results of the ICP-OES measurements conducted on both, the ternary master alloys and selected samples are listed in Table 1. As can be seen, the measured compositions of the alloys match well with the desired composition. Therefore, the desired compositions are used for labelling the samples throughout the article.

According to XRD measurements, all samples are single phase and show the Cu prototype crystal structure. The XRD patterns reveal no secondary phases or superlattice peaks. One XRD pattern is exemplified in Fig. 2(a), which is representative for all samples, despite the changing Bragg positions due to the change in lattice parameter. The lattice parameter of the samples is altered due to compositional changes and is found to be an average value of the lattice parameters of the elements

Table 1
Composition of selected samples obtained from ICP-OES.

Designation	Au / at %	Cu / at %	Ni / at%	Pd / at%	Pt / at%
CuPdPt		33.3 ±0.5		33.2 ±0.3	33.5 ±0.2
AuCuPd	33.7 ±0.3	33.4 ±0.3		32.9 ±0.2	
$Au_{2,5}Ni_{22,5}(CuPdPt)_{75}$	2.5±0.1	24.9 ±0.2	22.7 ±0.1	24.9 ±0.2	25.0 ±0.2
$Au_{7,5}Ni_{17,5}(CuPdPt)_{75}$	7.5±0.1	24.9 ±0.2	17.7 ±0.1	25.0 ±0.2	25.0 ±0.2
$Au_{15}Ni_{10}(CuPdPt)_{75}$	15.1 ±0.2	24.8 ±0.3	10.1 ±0.1	25.0 ±0.2	25.0 ±0.3
$Au_{25}(CuPdPt)_{75}$	25.1 ±0.2	24.9 ±0.2		25.0 ±0.2	25.0 ±0.3

weighted by their atomic concentration. In consequence, the lattice parameters of the $Au_xNi_{25-x}(CuPdPt)_{75}$ and $Ni_xPt_{25-x}(AuCuPd)_{75}$ series show a linear dependence on the compositional change (Fig. 2(b)). This is seen as additional evidence for the preservation of a single-phase microstructure. However, the experimental lattice parameters are slightly higher than the theoretical values calculated by Vegard's rule of mixtures but still show satisfying accordance (Fig. 2(c)).

In order to evaluate the chemical homogeneity at the nanoscale, some samples were further investigated by APT. This is done to rule out phase decomposition at the nm range. CuNiPdPt, AuCuPdPt, and AuCuNiPd, i.e. the first and last samples of the alloy series, were already investigated previously by APT [21]. The measurements confirm a random distribution of the elements at the nm range. Within the scope of this study, two additional alloys were investigated from both series, namely $Au_{15}Ni_{10}(CuPdPt)_{75}$ and $Ni_{15}Pt_{10}(AuCuPd)_{75}$. Fig. 3 shows the reconstructed APT tips and the concentration profiles. The reconstructed tips show a homogeneous distribution of the elements. The concentration profiles, however, suggest a slight gradient of some elements (Au, Ni, and Pt) along the longitudinal direction of the tip from top to bottom. This effect is attributed to measurement artefacts, which are explained in more detail in Appendix A3. Therfore, the element distribution is assumed to be homogeneous in the nm range. As a result, the thorough examination of the alloys under investigation by means of XRD and APT confirmed their single-phase characteristics. No indications on multi-phase constitution of the samples were detected within the limitations of the method. Furthermore, the APT analysis performed in the framework of the present study did not yield evidence for short-range oder (SRO) within the limitations of the method. The ion maps in Fig. 3 are not suitable for the assessment of SRO. The required analysis of Pearson coefficients and cluster search (frequently used in literature) were applied and no conclusive evidence for SRO was found. A reasonable analysis of SRO should be analysed by means of extended X-ray absorption fine structure (EXAFS) analysis, which is beyond the capabilities of the present study.

Fig. 4 shows the microstructure and the grain sizes *D* of the $Au_xNi_{25-x}(CuPdPt)_{75}$ and $Ni_xPt_{25-x}(AuCuPd)_{75}$ alloys. The BSE images reveal sole orientation contrast and absence of any atomic number contrast variation throughout the micro and mesoscale of the microstructures. Considering XRD on the macroscale, SEM-BSE on meso- and microscale as well as APT on nanoscale, chemical homogeneity of the samples is verified.

As the samples were in the recrystallized condition, only grain boundary strengthening could alter the strength besides the impact of solid solution strengthening representing the key aspect of the present study. Consequently, the analysis of grain size was conducted to demonstrate its impact on strength, enabling the consideration of the sole impact of solid solution strengthening on the strength.

While the grain sizes are comparably small across the investigated $Au_xNi_{25-x}(CuPdPt)_{75}$ samples, ranging from 24 to 64 μm with standard deviations up to 10 μm, they are larger for the different $Ni_xPt_{25-x}(AuCuPd)_{75}$ samples, i.e. the size ranges from 58 to 179 μm. Also, larger standard deviations are observed, i.e. up to 64 μm. The contribution of grain boundary strengthening is expected to be lower in the case of the $Ni_xPt_{25-x}(AuCuPd)_{75}$ alloys when compared to the $Au_xNi_{25-x}(CuPdPt)_{75}$ alloys due to the larger grain size of the former. To assess the effect of the grain size on the strength, the contribution of Hall-Petch strengthening

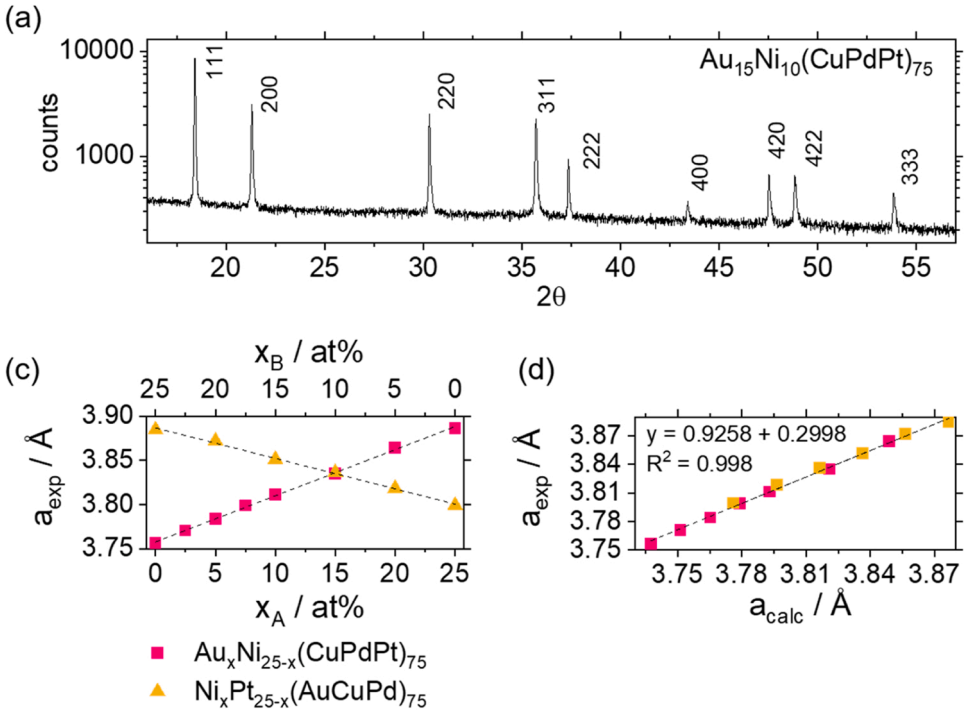

Fig. 2. (a) Representative XRD pattern of the $Au_{15}Ni_{10}(CuPdPt)_{75}$ alloy, (b) lattice parameter in dependency on the composition, and (c) experimental lattice parameter as a function of the lattice parameter calculated by Vegard's rule of mixtures.

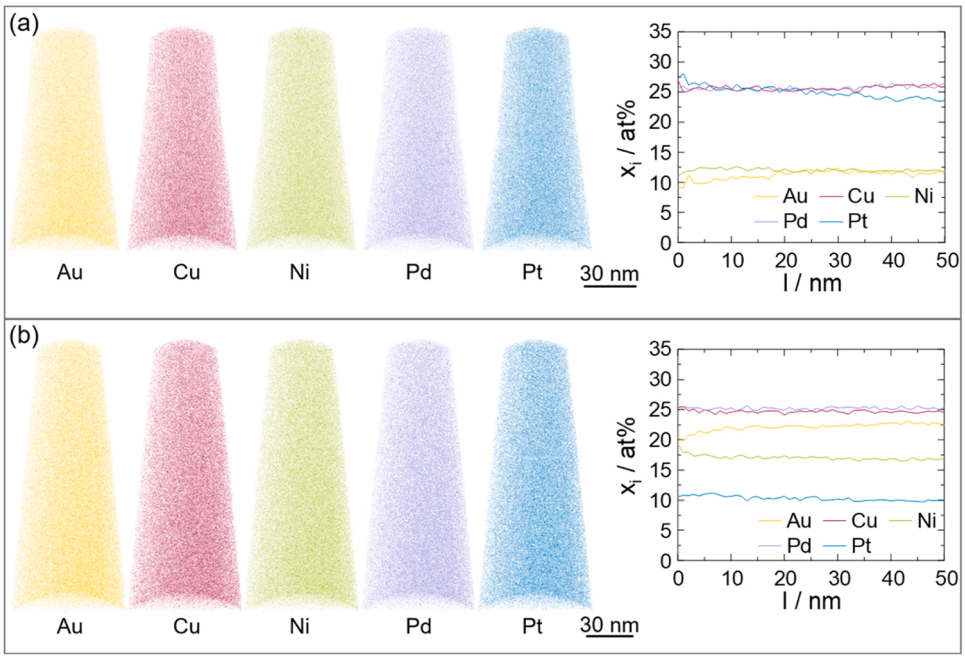

Fig. 3. Atom probe tomography measurements including the reconstructed tips showing 3 % of the detected ions, and concentration profiles along the longitudinal axis of the tip: (a) $Au_{15}Ni_{10}(CuPdPt)_{75}$ and (b) $Ni_{15}Pt_{10}(AuCuPd)_{75}$.

has been determined on two $Ni_xPt_{25-x}(AuCuPd)_{75}$ samples (x = 0 and 15). Grain growth was initiated at the temperature at which the samples were recrystallized before, while the time of grain growth was varied between 5 min and 120 h. The contribution of the grain boundary strengthening (also named Hall-Petch strengthening) to the total strength can be determined according to [27]:

$$\Delta\sigma_{c,HP} = \frac{k_y}{\sqrt{D}} \tag{4}$$

Herein, D is the grain size and k_y the Hall-Petch coefficient. The yield strength in dependence on the inverse square root of the grain size is plotted in Fig. 5.

The Hall Petch coefficient k_y and the offset yield strengths, which in the present case include the intrinsic strength σ_0 and the solid solution contributions to strength $\Delta\sigma_{c,ss}$ are listed in Table 2.

The Hall-Petch coefficients are lower than that determined for AuCuNiPdPt (675 MPa$\sqrt{\mu m}$) [18]. However, differences in grain sizes between 50 and 200 μm lead to a change in the yield strength of only 30 MPa (AuCuPdPt), and 23 MPa ($Ni_{10}Pt_{15}(AuCuPd)_{75}$), respectively. If the largest observed k_y of 675 MPa$\sqrt{\mu m}$ would be valid for all investigated samples the maximum deviation of the contribution of grain boundary strengthening to the total strength would be 38 MPa for the $Ni_xPt_{25-x}(AuCuPd)_{75}$ series and 53 MPa for the $Au_xNi_{25-x}(CuPdPt)_{75}$ series. These values being estimated assuming the largest possible influence of grain boundary strengthening are small when compared to the variation of the yield strength observed within the entire alloy series (~ 200 MPa), which in consequence is dominated by the variation in solid solution strengthening. The contribution arising from Hall-Petch strengthening is considered to have a minor influence on the total strength, only.

For the alloys under investigation, the yield strength σ_y can be expressed by the superposition of the intrinsic strength and the two relevant strengthening mechanisms. A superposition law in a general form [28] can read as:

$$\sigma_y = \sigma_0 + \sqrt[k]{\sum\nolimits_i \Delta\sigma_i^k} \tag{5}$$

Herein, $\Delta\sigma_i$ is representative for the contributions of solid solution strengthening $\Delta\sigma_{c,ss}$ and grain boundary strengthening $\Delta\sigma_{c,HP}$ to the yield strength. The exponent k is typically between 1 and 2. In the specific case, where the distances of obstacles for dislocation slip differ significantly for the strengthening mechanisms under investigation, or the sets of obstacles have seemingly different strengths, an exponent of $k = 1$ is justified. This holds for the present case, as the distances of the obstacles range from the average spacing of two solute atoms to the grain size, thus spanning more than five orders of magnitude.

Fig. 6 shows the mechanical properties of the $Au_xNi_{25-x}(CuPdPt)_{75}$ as well as the $Ni_xPt_{25-x}(AuCuPd)_{75}$ series in dependence of the composition. While Fig. 6(a) and (c) show the experimentally observed yield strength, its value reduced by the contribution of grain-boundary strengthening, the 7 % flow stress, and the microhardness for both series, Fig. 6(b) and (d) contrasts the experimental data with the predicted contribution of solid solution strengthening to the total strength. The experimental values show the same trend within each series. While hardness and strength are distinct properties, hardness is commonly correlated to the flow stress at a true plastic strain of 0.07 by a factor of approximately 3 (hardness value vs. flow stress in MPa) [29]. As already observed for the $A_x(BCED)_{100-x}$ series [21], the microhardness shows the same trend as the 7 % flow stress and the yield strength. This indicates a similar strain hardening behavior of all investigated alloys and a consistent description of changing solid solution strengthening irrespective of the quantity considered. Also, in the present case, the microhardness represents a suitable characteristic value for mapping the concentration-dependent mechanical properties, particularly the strength characteristics. It is worth noting that the microhardness is impervious to variations in grain size due to small indentation size and indentation positions off grain boundaries. This independence allows for a direct correlation between microhardness values and the values obtained from the model for solid solution strengthening, circumventing the necessity to consider grain-boundary strengthening. Nevertheless, the contribution of grain-boundary strengthening is low as discussed before and does not alter the observed behaviour.

In both alloy series, a clear discrepancy between the model and experiment can be observed (again irrespective of the experimental quantity considered). According to the model, the strength is supposed to show a parabolic development within the $Au_xNi_{25-x}(CuPdPt)_{75}$ series

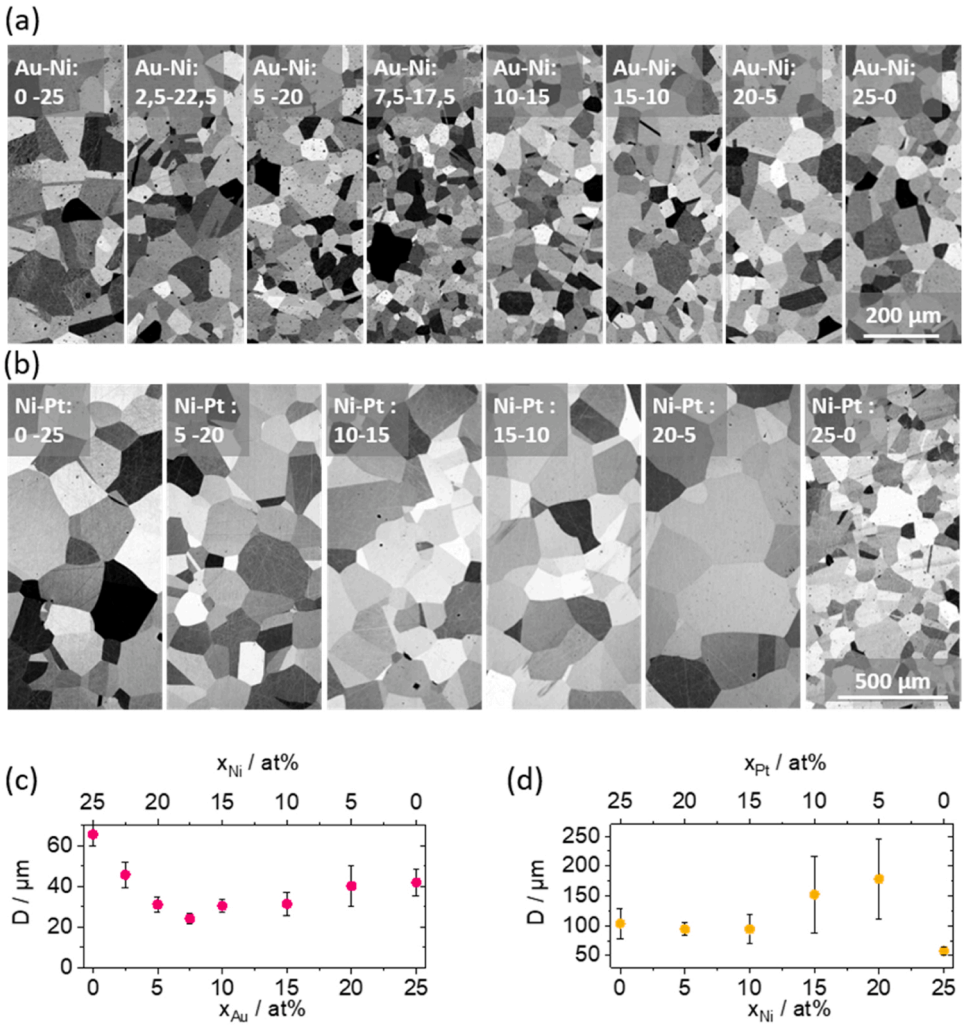

Fig. 4. BSE micrographs of (a) $Au_xNi_{25-x}(CuPdPt)_{75}$, and (b) $Ni_xPt_{25-x}(AuCuPd)_{75}$. Grain sizes are determined upon these images of (c) $Au_xNi_{25-x}(CuPdPt)_{75}$, and (d) of $Ni_xPt_{25-x}(AuCuPd)_{75}$.

with a maximum value at about 5 at% Au corresponding to 20 at% Ni (Fig. 6(b)). Instead, the experimental values reveal a maximum at the center and similar values at the beginning and the end of the series (Fig. 6(a)). A similar trend of the experimental values is found for the $Ni_xPt_{25-x}(AuCuPd)_{75}$ series (Fig. 6(c)), even though a monotonic, nearly linear course of the strength was expected (Fig. 6(d)).

Varvenne's model cannot be applied to describe the strength evolution of Au-Cu-Ni-Pd-Pt alloys. These findings are important, especially because there was a good agreement between experiment and model for the CoCrFeMnNi system. Only by investigating different alloy systems, the limits of existing models can be identified, and new approaches can be stimulated for their further development. In both presently investigated alloy series, a non-linear trend of the strength was observed with maximum values at the center of each series (526 MPa for $Au_{10}Ni_{15}(CuPdPt)_{75}$, and 581 MPa for $Ni_{15}Pt_{10}(AuCuPd)_{75}$, respectively). In contrast to the exchange of two elements against each other while these two elements are additionally alloyed to a three-element solid solution, a linear scaling was observed when a fifth element was added to a four-element solid solution (alloy series $A_x(BCED)_{100-x}$ ($0 \leq x \leq 20$) studied in Refs. [20,21]).

In Varvenne's model, the strength is based on solute-dislocation interactions and is, thus, independent of the number of elements in the alloy. Based on the assumption that the elements are randomly distributed on the same lattice site, an effective averaged matrix is defined, and each atom is considered as a solute. Thus, the strength is largely determined by the concentration-weighted mean-square misfit volume and the concentration-weighted shear modulus. However, in alloys based on Au-Cu-Ni-Pd-Pt, the relation seems to be different. The misfit parameter revealed a similar trend as the experimental yield strength for $Au_xNi_{25-x}(CuPdPt)_{75}$ alloys but shows a contradicting behaviour for $Ni_xPt_{25-x}(AuCuPd)_{75}$ alloys. The discrepancy cannot be explained by the changes in the shear modulus because a linear increase is expected in both series (see Fig. A4, Appendix A5). Within the $A_x(BCED)_{100-x}$ series, the development of the strength is also non-compliant to the development of the calculated misfit parameter within $Cu_x(AuNiPdPt)_{100-x}$, $Pd_x(AuCuNiPt)_{100-x}$, and $Pt_x(AuCuNiPd)_{100-x}$ [21]. These reasons are discussed for the observed discrepancy in the following: (i) The calculated misfit parameter does not adequately reflect the actual lattice stresses, (ii) the assumption of a random matrix is inadequate due to next-neighbor correlations, (iii) additional strengthening mechanisms occur that are not included in the model.

(i) In the Au-Cu-Ni-Pd-Pt system, the differences in atomic radii are much larger ($\Delta r_{max} = 32$ pm) than in the Co-Cr-Fe-Mn-Ni system ($\Delta r_{max} = 17$ pm) [10]. Due to the different atomic sizes, the lattice relaxation varies locally. In binary AuCu and AuNi alloys, it has been shown by X-ray absorption fine structure measurements that the small Ni and Cu atoms are further displaced from their positions compared to the large Au atoms. In contrast, the larger Au atoms are more confined to the regular lattice positions [30–32].

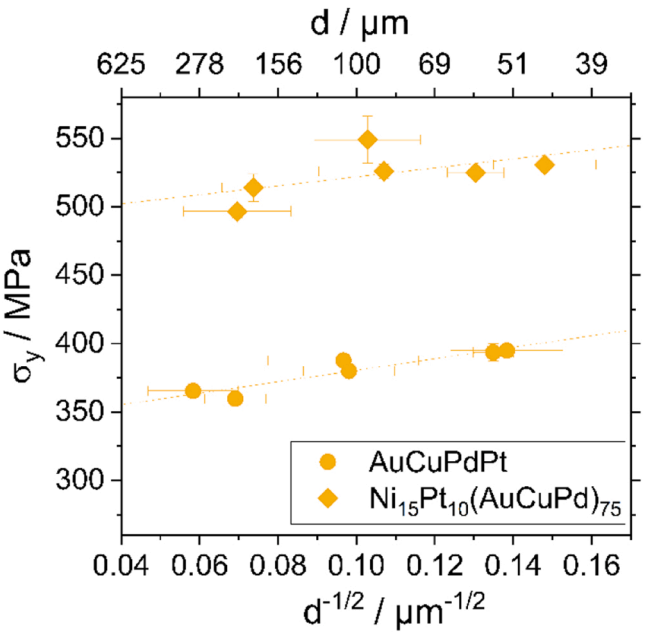

Fig. 5. Compressive yield strength in dependence on the grain size in AuCuPdPt and $Ni_{15}Pt_{10}(AuCuPd)_{75}$.

Table 2
Hall-Petch coefficient k_y and offset stress ($\sigma_0 + \Delta\sigma_{c,ss}$) of AuCuPdPt and $Ni_{15}Pt_{10}(AuCuPd)_{75}$ determined from the linear fits in Fig. 5.

	AuCuPdPt	$Ni_{10}Pt_{15}(AuCuPd)_{75}$
k_y/MPa•$\mu m^{1/2}$	420	328
$(\sigma_0 + \Delta\sigma_{c,ss})$ / MPa	339	489

Consequently, the lattice parameter is more determined by the large atoms, which is the reason for the insignificant positive deviation of the lattice parameter from Vegard's law (see Fig. 2 (c)). For the Ni-Ni distances in an AuNi alloy, Renaud et al. [30] determine a radial distribution function that is even comparable to an amorphous alloy. This means that the misfit depends not only on the differences between the atomic size of the individual elements and the (concentration-weighted) mean atomic size. The atomic size difference between the individual elements also seems to play a decisive role in the positional disorder. Consequently, the change in the misfit parameter caused by the addition or exchange of an element might not correlate with the actual change in the atomic spacings. In particular, the Goldschmid radii are depending on the environment. As this environment is subjected to spatial changes in multi-element alloys, a decent, size for an atom cannot be specified. The misfit volumes are calculated based on average atomic sizes. However, it is scientifically not sound in the present case to do so as the average atomic size has a large standard deviation and variance which would have to be considered as well. As a consequence, the meaningfulness of aa average value is limited. In both presently investigated alloy series, a small atom (Ni) is exchanged by a large atom (Au or Pt). The maximum strength is observed at the composition where both elements are contained in similar proportions. The combination of as many large and small atoms as possible seems to increase lattice misfit, which in consequence would raise the strength.

(ii) It is not clear whether the elements are truly randomly distributed on the lattice sites although the APT measurements confirmed the homogeneity of the microstructure at the nm level. However, this finding cannot unambiguously exclude preferred next-neighbor bindings within a few unit cells. In the close packed Cu prototype crystal structure, a small atom is presumably more likely surrounded by large atoms and vice versa. If such short-range ordering occurs, gliding of dislocations might lead to the creation of geometrical antiphase situations, which in turn would cause an additional contribution to the stress needed for dislocation slip. Besides the geometrical consideration, the pair enthalpy of mixing could be another indicator for preferred next-neighbor bindings. This approach was already used to explain segregating effects after certain heat treatments in AuCuNiPdPt and AuCuNiPt [18,19]. The influence of short-range order (SRO) on strength in high-entropy alloys is frequently discussed in literature and is mostly considered to increase strength [15, 33–36]. The investigations are mostly limited to the Co-Cr-Fe-Mn-Ni system, where no deviation from Varvenne's model is apparent. However, models have recently been developed that predict the occurrence of SRO and take into account the effect of solute-solute interactions [37,38]. In the future, this could make it possible to describe the strength evolution of Au-Cu-Ni-Pd-Pt alloys more accurately.

(iii) Regarding additional strengthening mechanisms, an interesting approach was derived by Zeng et al. [39]. Dislocation dynamics simulations were used to investigate the effect of local variations of the stacking fault energy (SFE) on strength. Because the spacings of partial dislocations were observed to differ [40,41], it was assumed that this could lead to dislocation pinning in regions where the SFE is high. The simulations of Zeng et al. [39] revealed a wavy shape of the partial dislocations. They could also show that the yield strength increases when the fluctuations of the SFE are enlarged. In contrast, Varvenne's theory assumes that the SFE has little effect on strength when the spacing of the partials is greater than seven times the Burgersvector. Thus, fluctuations in the SFE are not considered. Also, the concentration dependence and possible fluctuations of the dislocation line tension are not considered. The line tension parameter α was taken as 0.123 in analogy to the CrFeNi matrix case, which might be a poor approximation for Au-Cu-Ni-Pd-Pt alloys.

4. Conclusions

Two alloy series were prepared ($Au_xNi_{25-x}(CuPdPt)_{75}$, and $Ni_xPt_{25-x}(AuCuPd)_{75}$), consisting of single-phase alloys with low dislocation densities and low contributions of grain-boundary strengthening. These series are suitable to represent the concentration-dependent effect of solid solution strengthening. In this study, an experimental database of the mechanical properties was created for a multi-element alloy series in which two elements are exchanged by each other while they are alloyed to an equimolar three-element solid solution. This serves as a basis for the extension of models on solid solution strengthening. In pseudo-binary alloy series in the style of $A_x(BCED)_{100-x}$, a linear trend of the strength in dependence of the composition was measured. In contrast to this, a pseudo-ternary composition variation in the style of $A_xB_{25-x}(CDE)_{75}$ causes a non-linear trend with a maximum value at the center of the alloy series. Furthermore, in both alloy series, a discrepancy between the experiment and Varvenne's model was found. In most pseudo-binary and pseudo-ternary Au-Cu-Ni-Pd-Pt alloy series, no correlation between the key misfit parameter and strength could be observed. The hitherto summarized findings allow following conclusions:

(1) The prediction by the Varvenne model exhibits distinct deviations from the experimental observations in both alloy system that cannot be rationalized by considering the relevant macro-, micro- and nanoscale boundary conditions assumed in the model.
(2) The misfit parameter calculated according to the model of Varvenne is an inaccurate measure for alloys with large

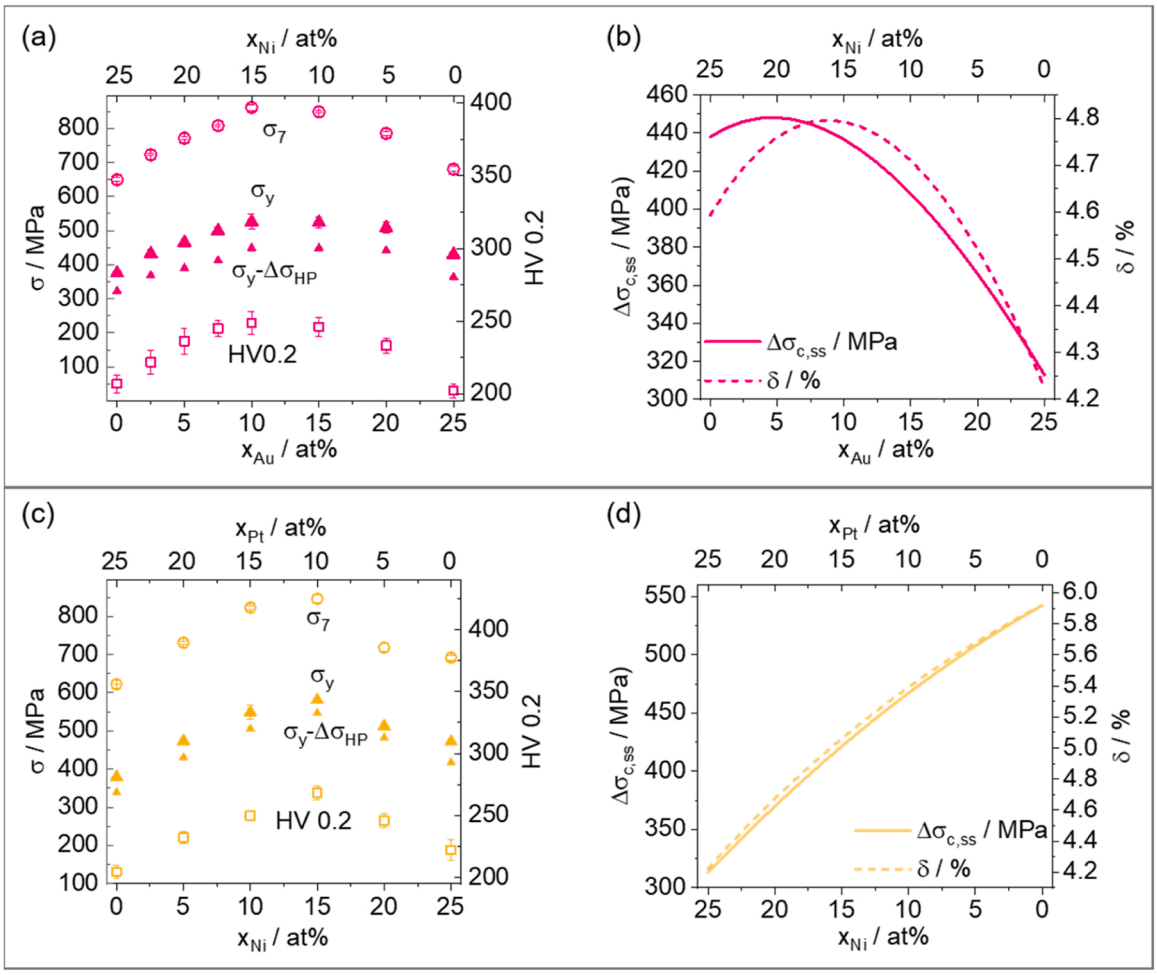

Fig. 6. (a), (c) Experimental data of yield strength (taken at 0.2 % total strain), its value reduced by the contribution of grain-boundary strengthening, 7 % flow stress, and microhardness vis-à-vis (b), (d) predicted contribution of solid solution strengthening to the total strength for $Au_xNi_{25-x}(CuPdPt)_{75}$ (b), and $Ni_xPt_{25-x}(AuCuPd)_{75}$ (d). The values of the given data are provided in Appendix A4.

differences in atomic sizes.Alternatively, the assumption of the random matrix is not fulfilled in Au-Cu-Ni-Pd-Pt-based alloys.

To gain a deeper understanding of the individual mechanisms of solid solution strengthening, further experimental studies as well as new theoretical approaches are required.

CRediT authorship contribution statement

S. Drescher: Investigation, Methodology, Formal analysis, Data Curation, Writing - Original Draft S. Seils: Investigation, Formal analysis, Writing – Review & Editing T. Boll: Investigation, Formal analysis, Writing – Review & Editing A. Kauffmann: Data Curation, Writing – Review & Editing M. Heilmaier: Conceptualization, Supervision, Writing - Review & Editing J. Freudenberger: Conceptualization, Methodology, Formal analysis, Writing - Original Draft, Supervision, Project administration, Funding acquisition.

Declaration of Competing Interest

The authors declare that they have no known competing financial interests or personal relationships that could have appeared to influence the work reported in this paper.

Data Availability

The raw data required to reproduce the present findings are available to download from https://doi.org/10.35097/1832.

Acknowledgments

This work was supported by the Deutsche Forschungsgemeinschaft (DFG) within the priority program *Compositionally Complex Alloys–High-Entropy Alloys (CCA-HEA)* (SPP 2006, grant no. FR 1714/7–2). This financial support is gratefully acknowledged. This work was partly carried out with the support of the Karlsruhe Nano Micro Facility (KNMF, www.knmf.kit.edu), a Helmholtz Research Infrastructure at Karlsruhe Institute of Technology (KIT, www.kit.edu). Furthermore, we would like to express our gratitude to D. Seifert, S. Donath, A. Voß, and A. Voidel for experimental support.

Appendix A1

Table A1
Lattice parameter and elastic constants of the elements. Data taken from [10].

Element	a / Å	G / GPa	E / GPa
Au	4.0782	27	78
Cu	3.6149	48	130
Ni	3.5241	76	200
Pd	3.8907	44	121
Pt	3.9242	61	168

Appendix A2. Calculated contribution of solid solution strengthening according to Varvenne's model [1]

The contribution of solid solution strengthening to the yield strength is visualized for all possible series where one element is exchanged by another. In (a), (c), (e), and (g) the contribution of solid solution strengthening is plotted in dependence of the composition. In (b), (d), (f), and (h) the contribution of solid solution strengthening is plotted in dependence on the misfit parameter δ. In two out of ten series, no clear relation is found between the contribution of solid solution strengthening and the misfit parameter: $Au_xCu_{25-x}(NiPdPt)_{75}$, and $Au_xNi_{25-x}(CuPdPt)_{75}$. Thus, two different strength values are calculated for the same misfit parameter. This seems implausible as the parelastic interactions differ depending on the misfit parameter and should predominate over the dielastic interactions. For the investigations of the study, one series with this anomaly was chosen ($Au_xNi_{25-x}(CuPdPt)_{75}$) and another with an expected linear relation ($Ni_xPt_{25-x}(AuCuPd)_{75}$).

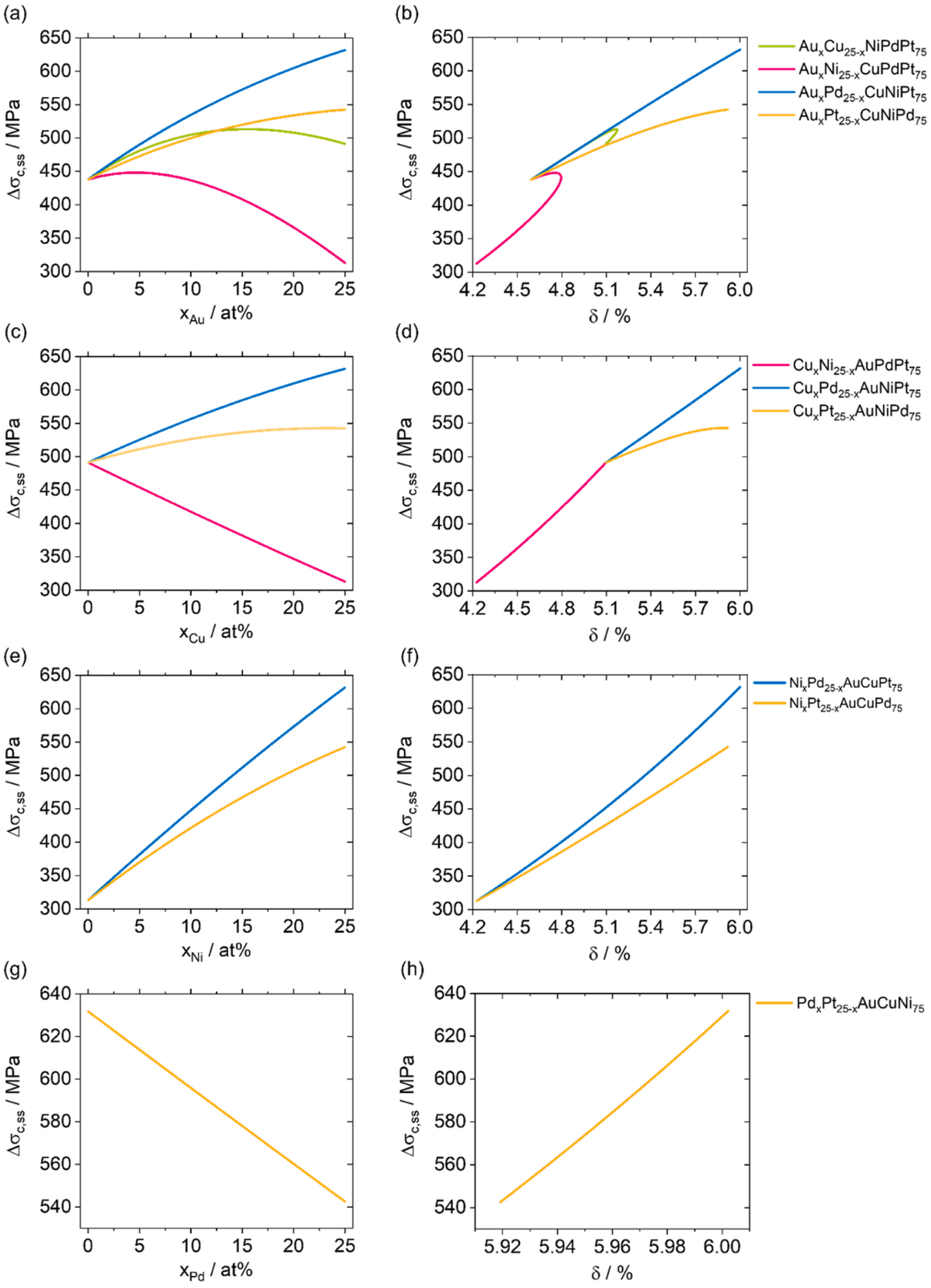

Fig. A1. Contribution of solid solution strengthening determined upon the model f Varvenne [1] (a), (c), (e), (g) in dependence on the composition, and (b), (d), (f), (h) in dependence on the misfit parameter δ.

Appendix A3. Atom probe tomography measurement

During APT of $Au_{15}Ni_{10}(CuPdPt)_{75}$, significant hydride formation occurred in some measurements, which impacts the concentration evaluation and is discussed in more detail in this section. In laser measurements, Au and Pt tend to recombine with H atoms from the atmosphere during

evaporation. As the peak of Au in the APT mass spectrum lies between the peaks of Pt, formation of Pt hydrides leads to peak overlapping and incorrect concentration determination. The H forming the hydrides stem mainly from H that was adsorbed to the shank of the tip from the chamber and diffused along the surface to the apex of the tip.The measurements were performed at a constant evaporation rate. Accordingly, the electrical field at the surface gradually decreased due to the increase in diameter of the sample tip, which changes the ratio of the different ionic charge states. Furthermore, due to the reduced flux (ions per area and time), the migration time of H to the apex of the tip increases towards the end of the measurement. Thus, the amount of detected hydrides increases as well. While the measurement of $Ni_{15}Pt_{10}(AuCuPd)_{75}$ was quite stable, the concentration profile in the tip was corrected for Au15Ni10(CuPdPt)75. The overlap of Ni hydrides and Cu and its hydrides was also considered. While the Cameca IVAS software allows to decompose peak overlaps for a given volume, for the presented graphs, this method is not feasible for individual intervals in the concentration profiles. For a natural isotope distribution of Au, one isotope (^{197}Au) is expected, while six natural isotopes of Pt exist, four of which are significant (^{190}Pt 0.01 %, ^{192}Pt 0.78 %, ^{194}Pt 32.9 %, ^{195}Pt 33.8 %, ^{196}Pt 25.2 %, ^{198}Pt 7.4 %). Since a peaks at 199 amu, 200 amu and 201 amu are obtained in the mass spectrum, we conclude on hydrides up to PtH_3. ^{197}Au is thus superimposed with ^{196}PtH, $^{195}PtH_2$ and $^{194}PtH_3$. To calculate the PtH_j contribution to the 197 amu peak, we ideally use a peak for correction with no overlaps. This is the case for $^{198}PtH_2$ and $^{198}PtH_3$. However, an additional overlap with $^{196}PtH_3$ is obtained for ^{198}PtH. To correct this overlap we calculate a corrected peak intensity from the natural abundances a (X) of the isotopes X with $I_{corr}(198PtH) = I(198PtH) - I(196PtH_3)\frac{a(198Pt)}{a(196Pt)}$. For $^{198}PtH_2$ and $^{198}PtH_3$, no overlaps occur and $I_{corr}(X) = I(X)$ is valid. With this correction, the expected contributions of all Pt hydrides from the Au-Peak can be subtracted and obtain the corrected Au concentration $I_{corr}(197Au) = I(197Au) - \sum_{j=1}^{3} I_{corr}(196PtH_j)\frac{a(197Au)}{a(196+jPt)}$. A similar correction was performed for the overlaps of the Cu isotopes at 63 amu and 65 amu with the Ni hydride isotopes. The impact on the calculated composition can be neglected. The considered overlaps are presented in Fig. A2 (a). The corrected and uncorrected results are visualised in Fig. A2 (b,c).

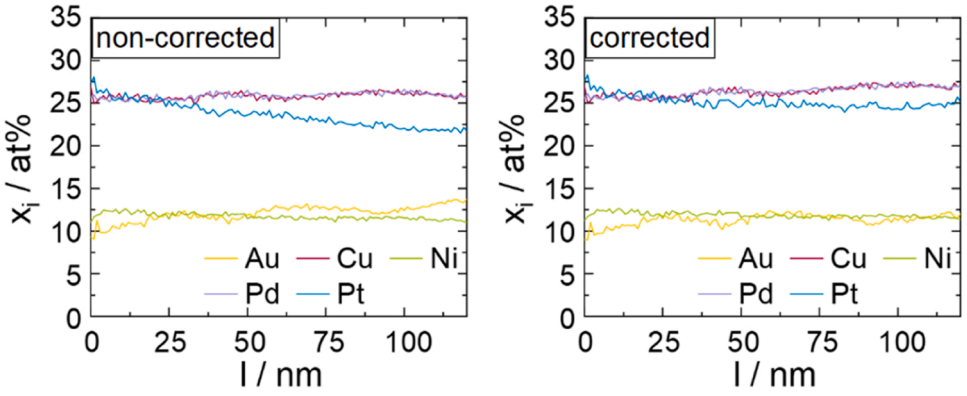

Fig. A2. Concentration profile of $Au_{15}Ni_{10}(CuPdPt)_{75}$ in the longitudinal direction (Ø=5 nm). The data were corrected by the overlap of the PtH_2 and PtH_3 hydrides. It can be shown that the increasing Au content and the decreasing Pt content is smoothed along the sample tip.

The corrected data shows a rather constant content of Au and Pt over the tip length. This strengthens the assumption that the line profile depends on the tip diameter and the associated measuring conditions. In addition, concentration profiles in the transversal direction were created for $Au_{15}Ni_{10}(CuPdPt)_{75}$ and $Ni_{15}Pt_{10}(AuCuPd)_{75}$ which are shown in Fig. A3. The profiles also show a constant composition of each element.

The Pearson coefficients clearly show that only the values for Au and Pt are increased in the $Au_{15}Ni_{10}(CuPdPt)_{75}$ sample (Table A2). In contrast, the values for Cu, Ni, and Pd are below 0.1, indicating a homogeneous distribution of these elements. In the $Ni_{15}Pt_{10}(AuCuPd)_{75}$ sample, the values for Au and Pt are smaller, but the coefficient for Ni is larger compared to the others. These values may be resulting from the hydride formation but cannot be corrected as performed for the composition. If certain elements segregated to clusters, other elements must be missing at these places. Accordingly, the Pearson coefficients for the other elements would necessarily also show increased values. An increased Pearson coefficient for just a single element in a complex solution is, thus, unlikely. In consequence, despite the measurement artifacts, the element distribution is assumed to be homogeneous as shown in the reconstructed sample tips of each element (Fig. 3).

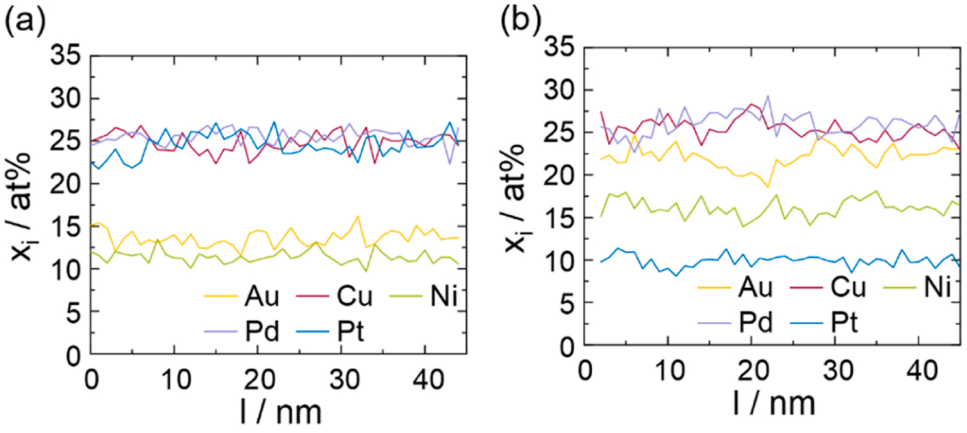

Fig. A3. Concentration profile along the transversal axis of the sample tip, diameter 10 µm. (a) $Au_{15}Ni_{10}(CuPdPt)_{75}$ and (b) $Ni_{15}Pt_{10}(AuCuPd)_{75}$.

Table A2
Pearson coefficient μ is a measure of the deviation of the theoretical binomial distribution and the experimental data of the elemental concentration distribution within the analysed volume of 100 ions.

Sample	μ(Au)	μ(Cu)	μ(Ni)	μ(Pd)	μ(Pt)
$Au_{15}Ni_{10}(CuPdPt)_{75}$	0.15	0.03	0.06	0.03	0.25
$Ni_{15}Pt_{10}(AuCuPd)_{75}$	0.08	0.04	0.13	0.02	0.17

Appendix A4. Mechanical data

Table A3
Experimental data of yield strength (σ_y), 7 % flow stress (σ_7), microhardness (HV 0.2) and the contributions of grain boundary strengthening (σ_{HP}) and dislocation strengthening ($\sigma_{disloc.}$) to the yield strength of $Au_xNi_{25-x}(CuPdPt)_{75}$ and $Ni_xPt_{25-x}(AuCuPd)_{75}$ alloys.

Sample	σ_y /MPa	σ_7/MPa	HV 0.2	σ_{HP}/MPa	$\sigma_{disloc.}$/MPa
$Au_0Ni_{25}(CuPdPt)_{75}$	375	649	207	52	<0.4
$Au_{2.5}Ni_{22.5}(CuPdPt)_{75}$	432	722	222	63	<0.4
$Au_5Ni_{20}(CuPdPt)_{75}$	465	771	236	75	<0.4
$Au_{7.5}Ni_{17.5}(CuPdPt)_{75}$	499	808	245	86	<0,4
$Au_{10}Ni_{15}(CuPdPt)_{75}$	526	861	249	77	<0.4
$Au_{15}Ni_{10}(CuPdPt)_{75}$	524	848	246	75	<0.4
$Au_{20}Ni_5(CuPdPt)_{75}$	508	785	233	66	<0.4
$Au_{25}Ni_0(CuPdPt)_{75}$	430	680	202	66	<0.4
$Ni_0Pt_{20}(AuCuPd)_{75}$	380	622	204	41	<1.2
$Ni_5Pt_{20}(AuCuPd)_{75}$	474	731	232	43	<2.1
$Ni_{10}Pt_{15}(AuCuPd)_{75}$	549	823	250	43	<1.6
$Ni_{15}Pt_{10}(AuCuPd)_{75}$	581	846	268	34	<1.1
$Ni_{20}Pt_5(AuCuPd)_{75}$	513	718	246	31	<1.6
$Ni_{25}Pt_0(AuCuPd)_{75}$	472	692	222	55	<1.5

The contribution of dislocation strengthening to the total yield strength was estimated upon a Williamson-Hall analysis while assuming that all lattice strains are causes by dislocations. Hence the given values can be considered as upper bounds and the total contribution of the dislocation strengthening is negligible as previously discussed.

Appendix A5. Shear modulus

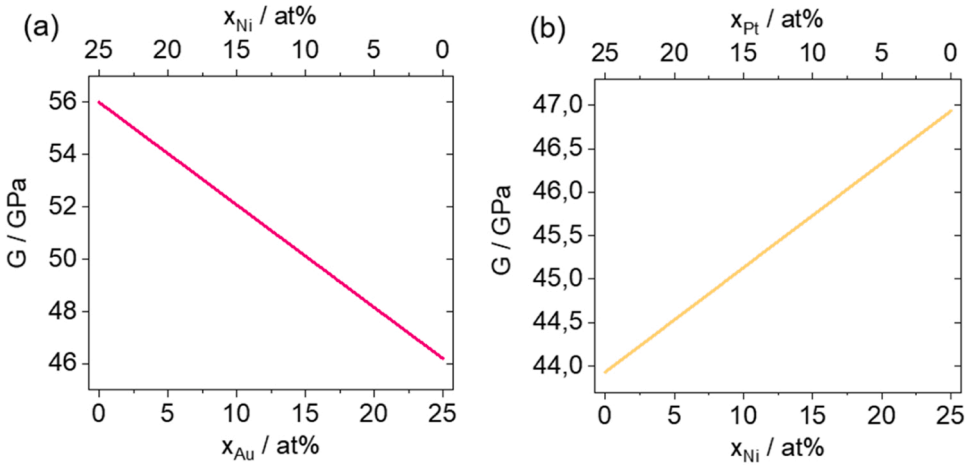

Fig. A4. Shear modulus (as calculated from the values of the elements upon a linear rule of mixture) of (a) $Au_xNi_{25-x}(CuPdPt)_{75}$, and (b) $Ni_xPt_{25-x}(AuCuPd)_{75}$ in dependence on the composition.

The shear modulus of the alloys is expected to change according to Vegard's rule of mixture. We proved this assumption of Varvenne [1] upon the AuCuNiPdPt alloy, which is not covered by the present study. We performed measurements with a torsional pendulum on a wire of the AuCuNiPdPt alloy. The resulty yield a Young's modulus of 51.7 ± 0.4 GPa, which is in agreement with the value as expected from a linear rule of mixture of the Young's moduli of the pure elements, i.e. 51.2 GPa (see Tab. A 1, Appendix A1).

References

[1] C. Varvenne, A. Luque, W.A. Curtin, Acta Mater. 118 (2016) 164, https://doi.org/10.1016/j.actamat.2016.07.040.
[2] J.-W. Yeh, S.-K. Chen, S.-J. Lin, J.-Y. Gan, T.-S. Chin, T.-T. Shun, C.-H. Tsau, S.-Y. Chang, Adv. Eng. Mater. 6 (2004) 299, https://doi.org/10.1002/adem.200300567.
[3] F. Otto, Y. Yang, H. Bei, E.P. George, Acta Mater. 61 (2013) 2628, https://doi.org/10.1016/j.actamat.2013.01.042.
[4] B. Cantor, I.T.H. Chang, P. Knight, A.J.B. Vincent, Mater. Sci. Eng.: A 375-377 (2004) 213, https://doi.org/10.1016/j.msea.2003.10.257.
[5] A. Gali, E.P. George, Intermetallics 39 (2013) 74, https://doi.org/10.1016/j.intermet.2013.03.018.
[6] F. Otto, A. Dlouhy, C. Somsen, H. Bei, G. Eggeler, E.P. George, Acta Mater. 61 (2013) 5743, https://doi.org/10.1016/j.actamat.2013.06.018.
[7] R. Labusch, Phys. Status Solidi (B) 41 (1970) 659, https://doi.org/10.1002/pssb.19700410221.
[8] R.L. Fleischer, Acta Metall. 11 (1963) 203, https://doi.org/10.1016/0001-6160(63)90213-X.
[9] C. Varvenne, G.P.M. Leyson, M. Ghazisaeidi, W.A. Curtin, Acta Mater. 124 (2017) 660, https://doi.org/10.1016/j.actamat.2016.09.046.
[10] Wolfram Research (2007), ElementData, Wolfram Language function, ⟨https://reference.wolfram.com/language/ref/ElementData.html⟩, ⟨https://www.webelements.com/⟩.
[11] D. Hull, D.J. Bacon. Introduction to Dislocations, 5th ed., Butterworth-Heinemann, 2011.
[12] Z. Wu, H. Bei, G.M. Pharr, E.P. George, Acta Mater. 81 (2014) 428, https://doi.org/10.1016/j.actamat.2014.08.026.
[13] G. Bracq, M. Laurent-Brocq, C. Varvenne, L. Perrière, W.A. Curtin, J.-M. Joubert, I. Guillot, Acta Mater. (2019), https://doi.org/10.1016/j.actamat.2019.06.050.
[14] T. Keil, D. Utt, E. Bruder, A. Stukowski, K. Albe, K. Durst, J. Mater. Res. 36 (2021) 2558, https://doi.org/10.1557/s43578-021-00205-6.
[15] Q. Ding, Y. Zhang, X. Chen, X. Fu, D. Chen, S. Chen, L. Gu, F. Wei, H. Bei, Y. Gao, M. Wen, J. Li, Z. Zhang, T. Zhu, R.O. Ritchie, Q. Yu, Nature 574 (2019) 223, https://doi.org/10.1038/s41586-019-1617-1.
[16] B. Yin, W.A. Curtin, Mater. Res. Lett. 8 (2020) 209, https://doi.org/10.1080/21663831.2020.1739156.
[17] C. Varvenne, W.A. Curtin, Scr. Mater. 142 (2018) 92, https://doi.org/10.1016/j.scriptamat.2017.08.030.
[18] F. Thiel, D. Geissler, K. Nielsch, A. Kauffmann, S. Seils, M. Heilmaier, D. Utt, K. Albe, M. Motylenko, D. Rafaja, J. Freudenberger, Acta Mater. 185 (2020) 400, https://doi.org/10.1016/j.actamat.2019.12.020.
[19] J. Freudenberger, D. Rafaja, D. Geissler, L. Giebeler, C. Ullrich, A. Kauffmann, M. Heilmaier, K. Nielsch, Metals 7 (2017) 135, https://doi.org/10.3390/met7040135.
[20] F. Thiel, D. Utt, A. Kauffmann, K. Nielsch, K. Albe, M. Heilmaier, J. Freudenberger, Scr. Mater. 181 (2020) 15, https://doi.org/10.1016/j.scriptamat.2020.02.007.
[21] J. Freudenberger, F. Thiel, D. Utt, K. Albe, A. Kauffmann, S. Seils, M. Heilmaier, Mater. Sci. Eng.: A 861 (2022) 144271, https://doi.org/10.1016/j.msea.2022.144271.
[22] Le Li, Z. Chen, S. Kuroiwa, M. Ito, K. Yuge, K. Kishida, H. Tanimoto, Y. Yu, H. Inui, E.P. George, Acta Mater. 243 (2023) 118537, https://doi.org/10.1016/j.actamat.2022.118537.
[23] B. Yin, S. Yoshida, N. Tsuji, W.A. Curtin, Nat. Commun. 11 (2020) 2507, https://doi.org/10.1038/s41467-020-16083-1.
[24] M.E. Straumanis, L.S. Yu, Acta Crystallogr. Sect. A 25 (1969) 676, https://doi.org/10.1107/S0567739469001549.
[25] D. Larson, T. Prosa, R. Ulfig, B. Geiser, T. Kelly, Local Electrode Atom Probe Tomography, Springer-Verlag, New York, 2013.
[26] M.P. Moody, L.T. Stephenson, A.V. Ceguerra, S.P. Ringer, Microsc. Res. Tech. 71 (2008) 542, https://doi.org/10.1002/jemt.20582.
[27] G. Gottstein, Physikalische Grundlagen der Materialkunde, Springer, Berlin Heidelberg, 2007.
[28] U. Kocks, A. Argon, M. Ashby, Prog. Mater. Sci. 1 (1975).
[29] K.L. Johnson, Contact mechanics, Cambridge Univ. Pr, Cambridge u.a, 1989.
[30] G. Renaud, N. Motta, F. Lançon, M. Belakhovsky, Phys. Rev. B 38 (1988) 5944, https://doi.org/10.1103/physrevb.38.5944.
[31] T.B. Wu, J.B. Cohen, Acta Metall. 31 (1983) 1929, https://doi.org/10.1016/0001-6160(83)90138-4.
[32] K. Lu, Z. Wu, J. Dong, X. Chen, Z. Fang, Jpn. J. Appl. Phys. 32 (1993) 631, https://doi.org/10.7567/jjaps.32s2.631.
[33] E. Antillon, C. Woodward, S.I. Rao, B. Akdim, T.A. Parthasarathy, Acta Mater. 190 (2020) 29, https://doi.org/10.1016/j.actamat.2020.02.041.
[34] S. Maiti, W. Steurer, Acta Mater. 106 (2016) 87, https://doi.org/10.1016/j.actamat.2016.01.018.
[35] F.X. Zhang, S. Zhao, K. Jin, H. Xue, G. Velisa, H. Bei, R. Huang, J.Y.P. Ko, D. C. Pagan, J.C. Neuefeind, W.J. Weber, Y. Zhang, Phys. Rev. Lett. 118 (2017) 205501, https://doi.org/10.1103/PhysRevLett.118.205501.
[36] D. Liu, Q. Wang, J. Wang, X.F. Chen, P. Jiang, F.P. Yuan, Z.Y. Cheng, E. Ma, X. L. Wu, Mater. Today Nano 16 (2021) 100139, https://doi.org/10.1016/j.mtnano.2021.100139.
[37] Y. Rao, W.A. Curtin, Acta Mater. 226 (2022) 117621, https://doi.org/10.1016/j.actamat.2022.117621.
[38] S. Nag, W.A. Curtin, Acta Mater. 200 (2020) 659, https://doi.org/10.1016/j.actamat.2020.08.011.
[39] Y. Zeng, X. Cai, M. Koslowski, Acta Mater. 164 (2019) 1, https://doi.org/10.1016/j.actamat.2018.09.066.
[40] T.M. Smith, M.S. Hooshmand, B.D. Esser, F. Otto, D.W. McComb, E.P. George, M. Ghazisaeidi, M.J. Mills, Acta Mater. 110 (2016) 352, https://doi.org/10.1016/j.actamat.2016.03.045.
[41] C. Varvenne, A. Luque, W.G. Nöhring, W.A. Curtin, Phys. Rev. B 93 (2016) 104201, https://doi.org/10.1103/physrevb.93.104201.